Two-pulse orientation dynamics and high-harmonic spectroscopy of strongly-oriented molecules

2014 J. Phys. B: At. Mol. Opt. Phys. 47 124030

(http://iopscience.iop.org/0953-4075/47/12/124030)

IOP Publishing Journal of Physics B: Atomic, Molecular and Optical Physics
J. Phys. B: At. Mol. Opt. Phys. **47** (2014) 124030 (13pp) doi:10.1088/0953-4075/47/12/124030

Two-pulse orientation dynamics and high-harmonic spectroscopy of strongly-oriented molecules

P M Kraus, D Baykusheva and H J Wörner

Laboratorium für Physikalische Chemie, ETH Zürich, 8093 Zürich, Switzerland

E-mail: woerner@phys.chem.ethz.ch

Received 10 December 2013, revised 24 March 2014
Accepted for publication 9 April 2014
Published 10 June 2014

Abstract

We present the detailed analysis of a new two-pulse orientation scheme that achieves macroscopic field-free orientation at the high particle densities required for attosecond and high-harmonic spectroscopies (Kraus *et al* 2013 arXiv:1311.3923). Carbon monoxide molecules are oriented by combining one-colour and delayed two-colour non-resonant femtosecond laser pulses. High-harmonic generation is used to probe the oriented wave-packet dynamics and reveals that a very high degree of orientation ($N_{up}/N_{total} = 0.73$–0.82) is achieved. We further extend this approach to orienting carbonyl sulphide molecules. We show that the present two-pulse scheme selectively enhances orientation created by the hyperpolarizability interaction whereas the ionization-depletion mechanism plays no role. We further control and optimize orientation through the delay between the one- and two-colour pump pulses. Finally, we demonstrate a complementary encoding of electronic-structure features, such as shape resonances, in the even- and odd-harmonic spectrum. The achieved progress makes two-pulse field-free orientation an attractive tool for a broad class of time-resolved measurements.

Keywords: orientation, high-harmonic generation, polar molecules, attosecond dynamics

(Some figures may appear in colour only in the online journal)

1. Introduction

A central goal of attosecond spectroscopy is the observation of electronic motion in the molecular frame [1]. The last decade has witnessed fundamental progress in the observation of electronic motion in atoms [2–4] and small molecules [5, 6]. We foresee an increasing focus of attosecond science on polar molecules which offer some of the most intriguing effects. These include charge migration [7–9] and the study of field-induced effects on electronic structure and dynamics because the coupling of the laser field with the permanent dipole moment of a polar molecule occurs in first-order. Finally, the extension of attosecond streaking [10, 11], RABITT (reconstruction of attosecond bursts by two-photon transitions) [12, 13] and tunnelling techniques [14, 15] to polar molecules could reveal fundamentally new physical insights into molecular-frame photoemission or tunnelling delays. All of the above-mentioned applications will only be possible if the molecules can be strongly oriented.

Other time-resolved techniques have already greatly benefited from aligning molecules in space [16]: measurements of photoelectron angular distributions of fixed-in-space CS_2 molecules revealed new insights into their vibronic dynamics [17]. Electron rescattering from aligned molecules provided information on the geometric structure of the investigated system [18, 19] and high-harmonic spectroscopy (HHS) of atoms and aligned molecules allowed the retrieval of electronic-structure information [20–23] and multi-electron effects [24–29] from the measured spectra. Recently, the measurement of valence-shell electronic wave packets in aligned molecules has been demonstrated [6].

Applying these techniques to the general case of polar molecules will greatly enhance the scope of these methods. However, molecular orientation has remained a much greater challenge than molecular alignment. Early

brute-force approaches of molecular orientation relied on the interaction of a dc field with a permanent molecular dipole moment [30] and were restricted to molecules with a large dipole moment. Subsequently, combinations of electrostatic fields and pulsed non-resonant fields were developed [31]. Further pertinent studies of molecular orientation include laser-field-free molecular orientation through the combination of a rapidly turned-off laser field and an electrostatic field [32]. The highest degrees of orientation reached so far have been achieved by aligning quantum-state selected molecules in combination with a weak dc field, either by adiabatic [33, 34] or impulsive [35] techniques. The use of non-resonant two-colour laser fields [36–38] showed a further promising route to molecular orientation, as it can be implemented in an all-optical setup without the need for additional electric fields or lossy state-selection stages. Nevertheless, the presence of an electric field in the form of a nanosecond laser pulse was a limitation, until the two-colour scheme could be successfully applied in an impulsive orientation experiment without the need of any additional fields [39]. The major limitation in the latter approach was the low degree of orientation. Nevertheless, as neither state-selection nor external electric fields were necessary, two-colour orientation enabled the first HHS-studies of oriented molecules [40, 41]. A recent analysis showed that impulsive two-colour orientation follows an ionization-depletion mechanism [42] resulting from the angular asymmetry of the strong-field ionization rates of polar molecules—very much like 'Lochfrass'-induced vibrational dynamics [43]—rather than an interaction of the laser electric field with the molecular hyperpolarizability [31].

The requirements for making molecular orientation broadly applicable to attosecond and HHSs can be summarized as follows: (i) high target densities are needed (typically $\geqslant 10^{15}$ cm^{-3}) owing to the weakness of attosecond pulses or the low efficiency of high-harmonic generation (HHG), respectively, (ii) external fields are undesirable because of their effect on the dynamics of the system or on the angular distributions of emitted photoelectrons and (iii) ionization of a large fraction of the sample (as in [40, 41]) is incompatible with the detection of charged particles and negatively impacts phase matching of the high-harmonic radiation. These three conditions were (to our knowledge) not met by any technique of molecular orientation reported prior to [44].

Here, we provide further details on this new scheme for molecular orientation [44] and extend it to orienting carbonyl sulphide (OCS) molecules. Our approach relies on the interaction of a one-colour and a delayed two-colour non-resonant femtosecond laser pulse with the molecular sample. This technique fulfils all three conditions listed above and improves the highest previously obtained degrees of field-free orientation by a factor of 3–4, reaching the level achievable by state-selection techniques. We implement the approach proposed in [45, 46] and optimize molecular orientation through quantum control of the odd- and even-J (rotational angular momentum quantum number) contributions to the rotational dynamics. We show through calculations that the present scheme creates orientation solely through the hyperpolarizability interaction as opposed to an ionization-depletion mechanism [42]. We probe the oriented rotational wave-packet dynamics by HHS which allows us to quantify the degree of orientation. Finally, we show how the high-harmonic spectra of oriented molecules can be simulated and used to retrieve electronic-structure information, preparing the ground for the reconstruction of attosecond charge migration in polar molecules [7–9]. The progress in orientation and the subsequent analysis allow us to identify a shape resonance in the even-harmonic spectrum of carbon monoxide (CO) and to reveal the influence of a sub-cycle Stark effect, which is a general phenomenon of polar molecules in strong laser fields.

This article is organized as follows: section 2 gives a detailed description of the experimental setup for two-pulse orientation. In section 3 we describe the theoretical model for calculating the oriented rotational wave-packet dynamics and for modelling the high-harmonic spectra. Section 4 presents the results on the orientation of carbon monoxide and carbonyl sulphide and section 5 contains the conclusions of this article.

2. Experimental setup

Experimentally, the investigated molecules are first exposed to a non-resonant 800 nm laser pulse, subsequently oriented by a two-colour 800 nm + 400 nm laser pulse and finally probed by HHG as depicted in figure 1. We refer to the timing of the maximum of the one-colour pump–pulse envelope as t_{p1}, that of the two-colour pump pulse as t_{p2} and that of the HHG probe pulse as t_{HHG}. We call the delay between the two pump pulses $\Delta t_1 = t_{p2} - t_{p1}$, the delay between the two-colour pump pulse and the probe pulse $\Delta t_2 = t_{HHG} - t_{p2}$ and the delay between the one-colour pump pulse and the probe pulse $\Delta t_{tot} = t_{HHG} - t_{p1}$. We use an amplified femtosecond titanium:sapphire laser system providing pulses centred at 800 nm with 8 mJ energy, 30 fs pulse duration and 1 kHz repetition rate. The two-colour laser pulse is generated in a 300 μm BBO crystal for frequency doubling tuned to a conversion efficiency of 25% in intensity, subsequently sent through two pieces of calcite (0.6 mm and 0.75 mm) for compensating the group and phase delays between the two colours and finally through a zero-order half-wave plate at 800 nm (acting as full-wave plate at 400 nm), which rotates the polarization of the 800 nm field into the polarization plane of the 400 nm field. The group and phase delay between the fundamental frequency and the second harmonic of the two-colour field are controlled by rotating one of the two calcite plates with a motorized rotation mount. The beam from which the one- and the two-colour pump pulses are generated propagates over a motorized and computer-controlled translation stage before being divided by a 50/50 beam splitter. We thus control both the one-colour-pump-to-probe delay Δt_{tot} and the two-colour-pump-to-probe delay Δt_2 with a single translation stage while leaving the delay Δt_1 between the two pump–pulses constant. After the beam splitter the orientation pulse (before generation of the two-color field) propagates along another motorized and computer-controlled translation stage, which allows control over the delay Δt_1 between the two pump pulses. The three beams are aligned parallel to each other and are non-collinearly focused into a gas target by a spherical mirror ($f = 50$ cm) with the two pump beams being vertically displaced by ± 7 mm relative to the HHG beam.

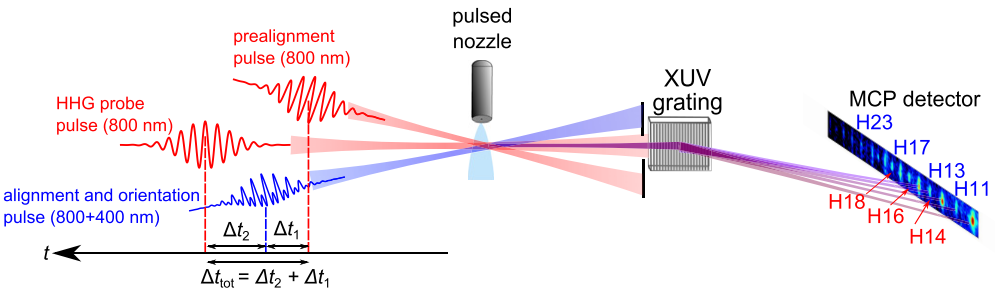

Figure 1. Scheme of the experimental setup for two-pulse orientation.

The gas target is a molecular beam generated by expansion of CO (neat) or OCS (10%, diluted in He) through a 500 μm diameter conical nozzle operated at 100 Hz with a backing pressure of 10 bar. The gas jet is intersected by the laser beams approximately 10 mm downstream of the nozzle to achieve the best possible cooling while at the same time preserving a sufficiently high particle density ($\sim 10^{17}$ cm^{-3}) for HHG and preventing the molecules from clustering. The peak intensities of the three pulses at their common focal point are estimated to be $5 \pm 2 \times 10^{13}$ W cm^{-2} for the one-colour pump pulse, $6 \pm 2 \times 10^{13}$ W cm^{-2} for the two-colour pump pulse and $2.2 \pm 0.1 \times 10^{14}$ W cm^{-2} for the HHG probe pulse in the case of CO. For OCS lower intensities were chosen due to the lower ionization potential: $2 \pm 1 \times 10^{13}$ W cm^{-2} for the one-colour pump pulse, $4 \pm 2 \times 10^{13}$ W cm^{-2} for the two-colour pump pulse and $1.3 \pm 0.1 \times 10^{14}$ W cm^{-2} for the HHG probe pulse. The high harmonics generated by the probe beam are spectrally dispersed in an XUV spectrometer consisting of a 250 μm wide entrance slit, a concave aberration-corrected grating (Shimadzu, 30-002) and a micro-channel-plate detector backed with a phosphor screen. A charge-coupled device camera records the spectral images and transfers them to a computer for further data processing.

3. Theory

3.1. Oriented rotational wave packets

We calculate the rotational wave-packet dynamics by solving the time-dependent Schrödinger equation (TDSE). The total Hamiltonian is separable into a time-independent part $\hat{H}_0$, which is approximated by the kinetic-energy operator of a rigid rotor, and a time-dependent part describing the cycle-averaged interaction of the laser fields with the molecule. The laser fields of the prealignment pulse $\varepsilon_1(t)$ and the two-colour orientation pulse $\varepsilon_2(t)$ are (atomic units are used throughout this section):

$$\begin{aligned}\varepsilon_1(t) &= G_1(t)\cos(\omega t)\\ \varepsilon_2(t) &= G_2(t)(\cos(\omega t) + \gamma\ \cos(2\omega t)),\end{aligned} \tag{1}$$

where $G_i(t)$ are the envelopes of the pulses centred at $t = 0$ and $t = \Delta t_1$ respectively, ω is the angular frequency of the fundamental laser field and γ is the ratio of the field strengths of the ω- and 2ω-components of the two-colour field. The cycle-averaged coupling of the electric field to the polarizability anisotropy $\Delta\alpha$ of a linear molecule is expressed by the potential term

$$\hat{V}_{\rm pol}(t) = -\tfrac{1}{4}G^2(t)(\Delta\alpha\cos^2\theta + \alpha_\perp), \tag{2}$$

where the action of the one-colour pump pulse $G_1(t)$ and the two-colour pulse $G_2(t)$ are evaluated sequentially. $\alpha_\perp$ is the component of the polarizability tensor perpendicular to the molecular axis and θ is the angle between the molecular axis and the polarization axis of the laser field.

The effect of the asymmetry of the laser field is incorporated in the cycle-averaged hyperpolarizability interaction (contributing to orientation), which represents the coupling of the laser field to the hyperpolarizability tensor β:

$$\hat{V}_{\rm hyp}(t) = -\tfrac{1}{8}\gamma G_2^3(t)[(\beta_{zzz} - 3\beta_{xxz})\cos^3\theta + 3\beta_{xxz}\cos\theta], \tag{3}$$

where β_{zzz} and β_{xxz} are components of the hyperpolarizability tensor. The ionization-depletion interaction is incorporated as a loss channel by means of an imaginary potential term [42]

$$\hat{V}_{\rm ion}(t) = -\frac{\rm i}{2}\Gamma(\theta, t), \tag{4}$$

which is approximately separable into an angle- and a time-dependent part

$$\Gamma(\theta, t) = \Gamma(\theta)K(t). \tag{5}$$

$\Gamma(\theta)$ denotes the angular variation of the ionization rate. $K(t)$ denotes the time-dependence of the ionization rate, which is

$$K(t) = \exp\left(-\tfrac{2}{3}(2I_{\rm p})^{3/2}(|\varepsilon(t)|^{-1} - |E_{\rm ref}|^{-1})\right), \tag{6}$$

where the effect of $\varepsilon_1(t)$ and $\varepsilon_2(t)$ is again evaluated sequentially. $E_{\rm ref}$ denotes the electric-field strength at which $\Gamma(\theta)$ was calculated. The wave function $\Phi_{J_0M_0}(t)$ prepared by the interaction of the laser pulse with the molecule in a pure initial state corresponding to the rotational angular momentum quantum number J_0 and its projection quantum number M_0 on a space-fixed axis defined by the polarization of the laser field can be expanded in the linear rigid rotor basis

$$|\Phi_{J_0M_0}(t)\rangle = \sum_J C_J^{J_0M_0}(t)\,|JM_0\rangle\,. \tag{7}$$

The rigid rotor basis $\langle\theta, \phi|JM\rangle = Y_J^M(\theta, \phi)$ is represented by spherical harmonics with θ and ϕ being the spherical-angle coordinates describing the spatial orientation of the molecular axis. Averaging over the thermal ensemble is performed by writing the density matrix of the system as a sum over the pure

Table 1. Molecular parameters for CO.

Parameter	Value	Parameter	Value
I_p	14.014 eV [51]	β_{xxz}	7.96 au [52]
B	1.93128 cm^{-1} [51]	β_{zzz}	28.91 au [52]
$\Delta\alpha$	3.594 au [52]		

Table 2. Molecular parameters for OCS.

Parameter	Value	Parameter	Value
I_p	11.185 eV [53]	β_{xxz}	−59.1 au [54]
B	0.203 cm^{-1} [54]	β_{zzz}	−45.0 au [54]
$\Delta\alpha$	27.15 au [54]		

states evolved from the initially populated levels

$$\rho(t) = \sum_{J_0 M_0} p_{J_0} \left|\Phi_{J_0 M_0}(t)\right\rangle \left\langle\Phi_{J_0 M_0}(t)\right|, \tag{8}$$

where the factor $p_{J_0} = (2J_0 + 1)\exp\left(-\frac{E_{J_0}}{k_B T}\right)/Q$ accounts for the initial thermal population, $E_{J_0} = BJ_0(J_0 + 1)$ are the eigenenergies of the system, T is the temperature, Q the rotational partition function and k_B the Boltzmann constant. The resulting TDSE consists of a system of coupled ordinary differential equations and is solved for each value of $C_J^{J_0 M_0}$ in a J-basis up to $J = 24$ (CO) or 35 (OCS) employing a fourth-order Runge–Kutta method. Subsequently, thermal averaging is performed over all significantly populated states (we chose all states which contribute 0.01% or more to the total population).

The calculations on CO used the strong-field ionization rate given in [42], which was calculated with the time-dependent mixed orbital and grid method [47] in the single-channel approximation. For OCS the strong-field ionization rate was obtained within the weak-field asymptotic theory (WFAT) [48, 49] and taken from [50]. Within the WFAT, the ionization rate is decomposed into a sum of weighted structure factors $G^{n_\xi m}$ representing ionization channels with different parabolic quantum numbers n_ξ and m. We used the structure factors G^{00} and G^{01} as given in [50]. The remaining relevant parameters for CO and OCS are given in tables 1 and 2.

3.2. High-harmonic generation from oriented molecules

We calculate the high-harmonic spectra of linear molecules by factorizing the high-harmonic emission dipole in the frequency domain into the contributions from strong-field ionization with the rate $I_{\text{ion}}(\theta)$, propagation with the amplitude a_{prop}, and the photorecombination dipole $d_{\text{rec}}(\Omega, \theta)$. This product is coherently averaged over the molecular axis distribution $A(\theta)$:

$$\mathrm{d}(\Omega) \propto \int_{\theta=0}^{\pi} A(\theta)\sqrt{I_{\text{ion}}(\theta)}\, a_{\text{prop}}(\Omega, \theta)\, \mathrm{d}_{\text{rec}}(\Omega, \theta) \sin\theta \,\mathrm{d}\theta. \tag{9}$$

The strong-field ionization rate $I_{\text{ion}}(\theta)$ is taken from the literature as discussed in the previous section. Ω is the angular frequency of the emitted high-harmonic radiation. The contribution from the propagation step a_{prop} is calculated in the strong-field approximation [55] with an additional, alignment-dependent phase factor arising from the Stark effect [56, 57]

$$\phi_{\text{Stark}}(\theta) = \mu \frac{E_0}{\omega} \cos\theta \left(\sin(\omega t_r) - \sin(\omega t_i)\right), \tag{10}$$

where t_r and t_i are the recombination and ionization times of the continuum electron at a given photon energy, which can be calculated within the three-step model [58] and μ is the permanent dipole moment of the ionized orbital. In evaluating equation (10), care must be taken to define μ and the coordinates of the electron in a consistent coordinate system. The photorecombination dipole moments for CO were calculated with EPOLYSCAT [59, 60] from single-hole configurations of the neutral molecule for the experimental bond length with a correlation-consistent polarized valence-triple-zeta (cc-pVTZ) basis set.

We now describe the calculation of high-harmonic spectra of an oriented sample, as it was first done in [40], and start by investigating the generation mechanism of the even and odd harmonic orders. Orientation breaks the inversion symmetry of the investigated molecular ensemble and therefore increases the periodicity of the HHG process from half an optical cycle to a full cycle. In two consecutive half cycles of the laser field, different high-harmonic emissions therefore occur and interfere, giving rise to both even and odd harmonics, as illustrated in figure 2(a). The electric field $E(\Omega)$ of the emission from two adjacent half cycles, normalized to one half cycle, is

$$E(\Omega) = \tfrac{1}{2}(d_1(\Omega) - d_2(\Omega)\exp(-\mathrm{i}\Omega T/2)), \tag{11}$$

where the minus sign is a consequence of the odd symmetry of the dipole operator and the phase factor $\exp(-\mathrm{i}\Omega T/2)$ accounts for the emission delay of half a period ($T = 2\pi/\omega$) at a given photon angular frequency $\Omega = q\omega$ for the harmonic order q. For the odd and even harmonics we thus obtain

$$E_{\text{odd}}(\Omega) = \tfrac{1}{2}(d_1(\Omega) + d_2(\Omega)) \tag{12}$$

$$E_{\text{even}}(\Omega) = \tfrac{1}{2}(d_1(\Omega) - d_2(\Omega)). \tag{13}$$

The odd harmonics thus correspond to the sum of electric fields emitted in adjacent half cycles, while the even harmonics correspond to their difference [40, 41, 61].

This mechanism was experimentally demonstrated in [40] by varying the delay between the ω- and 2ω-components of the two-colour orientation pulse, thus modifying the asymmetry of the laser electric field which is responsible for the orientation. The integrated harmonic intensity was measured as a function of the two-colour delay for a pump–probe delay corresponding to maximal orientation. The even-harmonic emission was found to be perfectly controlled through the two-colour delay (figure 2(c)), meaning that no even-harmonic emission is observed for a symmetric electric field while it is maximized for a maximal asymmetry of the field. In contrast, the intensity of the odd harmonics (shown for harmonic 9, panel (b)) remains unchanged when the two-colour delay is varied. Hence an oriented system constitutes a molecular interferometer for the harmonic emission of the two different sides of the electron recombination and thus provides side-sensitivity to HHS. This description holds for multi-cycle fields, but naturally breaks down for few- to single-cycle fields, where the harmonic structure of the spectrum is lost. In this case, spectra for recombination from a single side of the molecule could be obtained, provided that the molecule is strongly oriented. The present work opens such perspectives.

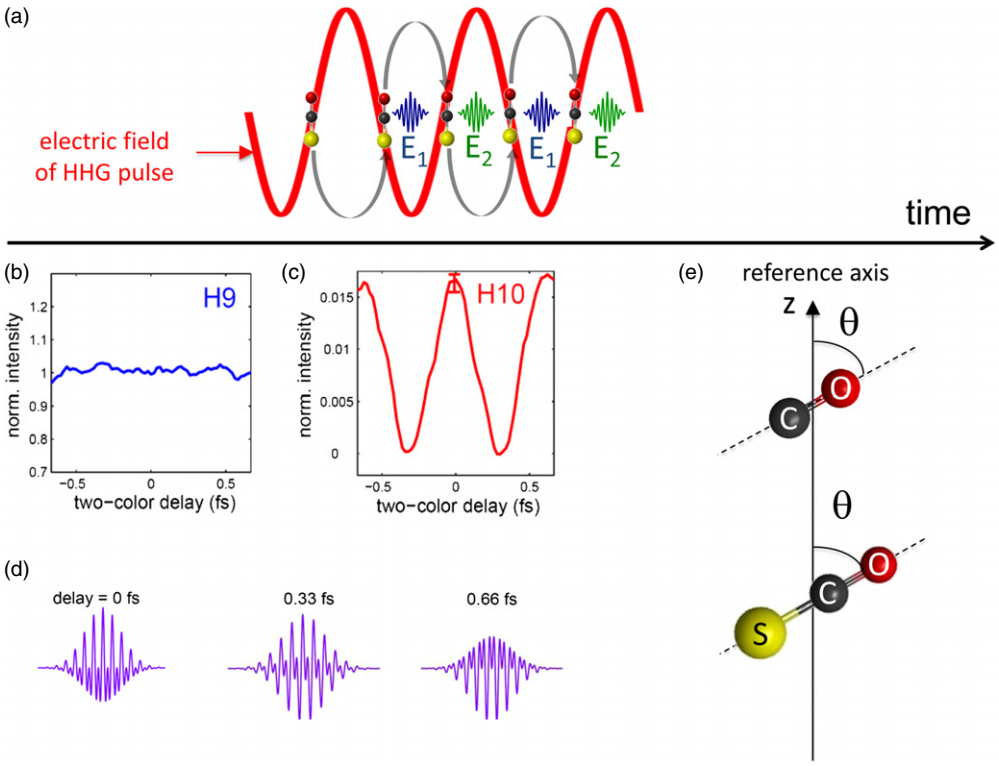

Figure 2. Illustration of HHG from oriented molecules. (a) Harmonic emission in adjacent half cycles from oriented molecules leads to the emission of different electric fields due to the different recollision sides. (b) Absence of modulation of the ninth harmonic order as a function of the two-colour delay. (c) Modulation of the tenth harmonic order as a function of the two-colour delay. The data in (b) and (c) are taken from [40]. (d) Schematic representation of the electric field of the two-colour pump pulse for three exemplary two-colour delays assuming $\gamma = 1$. (e) Definition of the axis system, the reference axis being either the polarization of the orientation pulse or that of the HHG pulse. (b), (c) and (d) reproduced with permission from [40]. Copyright 2012 American Physical Society.

Transferring this information to a partially aligned and oriented sample, we conclude that the emission from those half cycles where the electron excursion takes place to the positive side of the z-axis (according to figure 2(e)) is given by

$$d_1(\Omega) \propto \int_{\theta=0}^{\pi} A(\theta)\sqrt{I_{\mathrm{ion}}(\theta)}a_{\mathrm{prop}}(\Omega,\theta)d_{\mathrm{rec}}(\Omega,\theta)\sin\theta\,\mathrm{d}\theta, \tag{14}$$

and the emission of the opposite half cycles is

$$d_2(\Omega) \propto \int_{\theta=0}^{\pi} A(\theta)\sqrt{I_{\mathrm{ion}}(\pi-\theta)}a_{\mathrm{prop}}(\Omega,\pi-\theta) \times d_{\mathrm{rec}}(\Omega,\pi-\theta)\sin\theta\,\mathrm{d}\theta. \tag{15}$$

A simple change of variables ($\theta' = \pi - \theta$) in equation (15) leads to

$$d_2(\Omega) \propto \int_{\theta'=0}^{\pi} A(\pi-\theta')\sqrt{I_{\mathrm{ion}}(\theta')}a_{\mathrm{prop}}(\Omega,\theta') \times d_{\mathrm{rec}}(\Omega,\theta')\sin\theta'\,\mathrm{d}\theta'. \tag{16}$$

As a consequence, the odd-harmonic emission (equation (12)) is predicted by using equation (9) with a symmetrized axis distribution

$$A_{\mathrm{odd}}(\theta) = \tfrac{1}{2}(A(\theta) + A(\pi-\theta)), \tag{17}$$

whereas the even-harmonic emission (equation (13)) is calculated accordingly with an anti-symmetrized axis distribution

$$A_{\mathrm{even}}(\theta) = \tfrac{1}{2}(A(\theta) - A(\pi-\theta)). \tag{18}$$

We note that A_{even} can adopt negative values which account for the negative sign appearing in equation (13).

Accurate calculations of *oriented* axis distributions $A(\theta) = A_{\mathrm{ori}}(\theta)$ currently represent a significant challenge, because orientation is in general the result of a complex interplay of ionization-depletion [42] and hyperpolarizability [31] interactions. The contribution of the ionization-depletion mechanism is particularly challenging to model because the calculation of strong-field ionization rates of polar molecules is an active field of research with results that differ qualitatively, e.g. for CO molecules [42, 49, 62, 63].

In the present article, as in [40], we therefore only rely on calculating aligned axis distributions A_{ali} and circumvent the necessity of calculating A_{ori} in the following way. We solve the TDSE including only the polarizability interaction (equation (2)) and extract an aligned axis distribution $A_{\mathrm{ali}}(\theta)$ that we parameterize as follows [64]:

$$A_{\mathrm{ali}}(\theta) = N(1 + a/\sqrt{\cos^2\theta + b^2\sin^2\theta}), \tag{19}$$

where a and b are parameters that are adjusted to reproduce the calculated axis distribution [27] and N is a normalization constant. The axis distributions that we use to calculate even- and odd-harmonic spectra within this simplified framework are thus

$$\begin{aligned} A_{\mathrm{even}}(\theta) &= -A_{\mathrm{ali}}(\theta)\,\eta\,\mathrm{sgn}(\pi/2-\theta), \\ A_{\mathrm{odd}}(\theta) &= A_{\mathrm{ali}}(\theta), \end{aligned} \tag{20}$$

where the degree of orientation η is determined by comparing the measured and calculated high-harmonic spectra in a

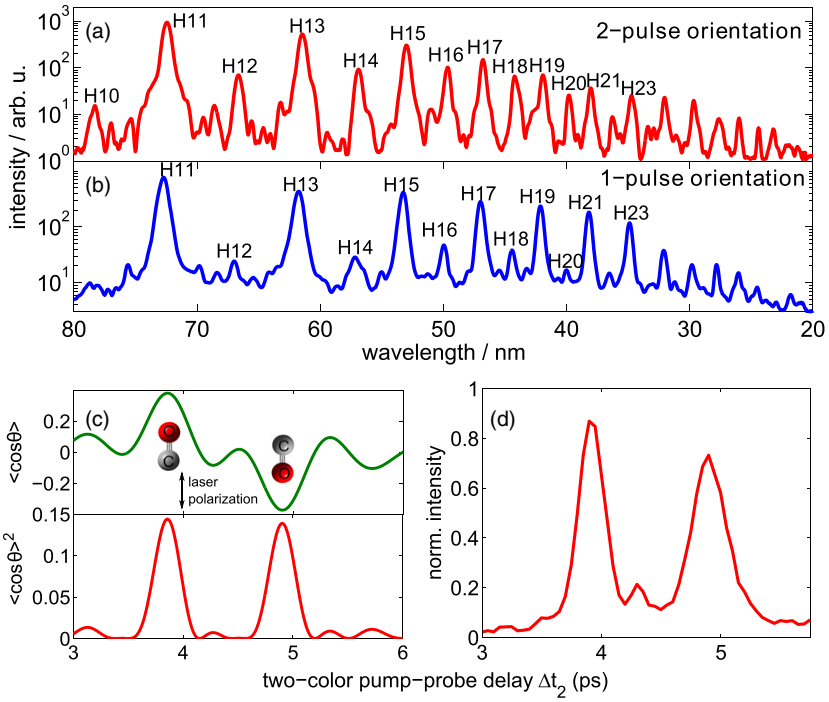

Figure 3. High-harmonic spectra of oriented CO molecules. (a) Spectrum of CO oriented with the two-pulse scheme. (b) Spectrum of CO obtained with the one-pulse orientation scheme. The even-harmonic emission is weaker by a factor of ∼9 compared to panel (a). (c) Calculated time evolution of $\langle\cos\theta\rangle$ (upper panel) and $\langle\cos\theta\rangle^2$ (lower panel) for the two-pulse scheme. (d) Measured integrated intensity of the 18th harmonic order as a function of the two-colour-pump-to-probe delay Δt_2 for the two-pulse scheme. The figure is adapted from [44].

single parameter fit, as was carried out in [40]. The degree of orientation obtained in this way is defined as $\eta = (N_{\rm up} - N_{\rm down})/(N_{\rm up} + N_{\rm down})$ ($N_{\rm up}$ and $N_{\rm down}$ denote the number of molecules pointing up or down along the pump–pulse polarization, respectively). Another commonly used measure for the degree of orientation (see e.g. [33]) is $\zeta = N_{\rm up}/(N_{\rm up} + N_{\rm down})$. The relation between the two quantities is $\zeta = (\eta + 1)/2$.

4. Results

4.1. Oriented wave-packet dynamics

Figure 3 compares high-harmonic spectra of oriented CO molecules obtained either by the two-pulse scheme described in section 2 (panel (a)) or by a one-pulse scheme in which the prealignment pulse was omitted (panel (b)). Besides the appearance of the commonly-observed odd-harmonic orders, even-harmonic emission is observed in both spectra because the molecular orientation breaks the inversion symmetry of the molecular ensemble. The even-harmonic orders emitted after orientation with the two-pulse scheme are significantly enhanced (approximately by a factor of 9) compared to the one-pulse scheme. Thus, the molecular orientation in the two-pulse scheme is dramatically enhanced as compared to the one-pulse scheme. In the two-pulse scheme the delay Δt_1 between the one- and two-colour pump pulses was set to 2.25 ps (corresponding to $0.26\,T_{\rm rot}$) and the high-harmonic spectrum was recorded with a delay of $\Delta t_2 = 3.90$ ps (corresponding to $0.45\,T_{\rm rot}$) [44]. In the one-pulse scheme the orientation was probed at a delay of 8.85 ps (corresponding to $1.03\,T_{\rm rot}$). Apart from the different delays, the remaining experimental parameters were the same for the spectra shown in figures 3(a) and 3(b), i.e. they were recorded using the same intensities for the two-colour pump and probe pulses and for the same backing pressures and further settings determining the cooling of the sample. The weak features observed between the even and odd harmonics arise from the second-order of the spectrometer grating (e.g. the two small peaks symmetrically arranged around H11 in panel (b)) or a background caused by the non-collinear pump pulses although care was taken to minimize this contribution.

We now turn to the evolution of the even-harmonic intensities as a function of Δt_2 for the two-pulse scheme. The calculated expectation values of $\langle\cos\theta\rangle$ and $\langle\cos\theta\rangle^2$ are shown in the upper and lower panels of figure 3(c), respectively. The measured time evolution of the integrated intensity of the 18th harmonic order (27.9 eV) normalized to the next higher odd-harmonic order (harmonic 19, 29.4 eV) is shown in figure 3(d). The normalized intensity reaches a value close to 0.9, reflecting the fact that H18 is nearly as intense as H19. The temporal evolution of H18 reveals two main maxima separated by approximately 1 ps. These two maxima arise from a global maximum and a global minimum in the time evolution of $\langle\cos\theta\rangle$ (see upper panel of figure 3(c)) and thus correspond to the two possible orientations of the molecule. This property makes the present two-pulse scheme for molecular orientation attractive for all molecular-side-resolved experiments, as both possible orientations of the molecule are available within a simple delay scan without the need for rotating the polarization of the pump or the probe pulse. The time evolution of the even-harmonic emission is well represented by $\langle\cos\theta\rangle^2$ (lower panel

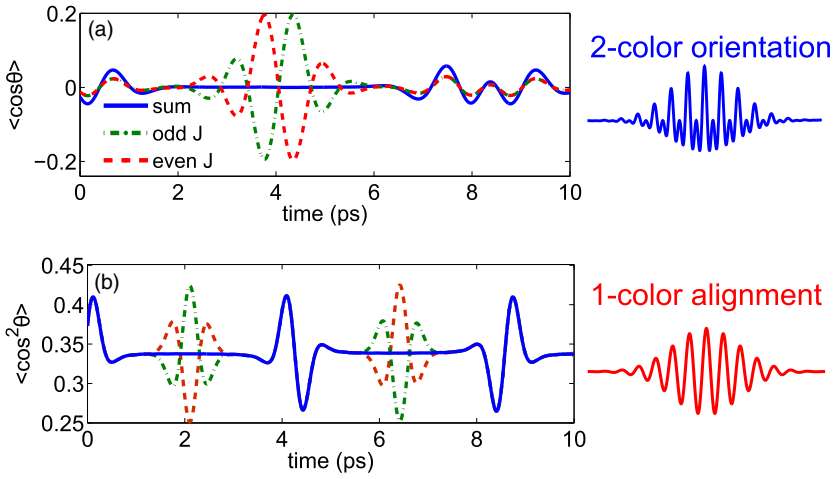

Figure 4. Illustration of the concepts of two-pulse orientation by calculated values of alignment and orientation parameters for CO. (a) Calculated evolution of the odd- and even-J contributions to the oriented wave-packet dynamics and their sum measured by $\langle \cos\theta \rangle$. Although no net orientation is obtained, the odd- and even-J contributions show the strongest orientation at the rotational half revival (around 4.3 ps). (b) Calculated time evolution for the odd- and even-J contributions to the aligned wave-packet dynamics and their sum measured by $\langle \cos^2\theta \rangle$. The odd-$J$ contributions align at the rotational quarter revival (2.15 ps) and can thus be oriented more strongly than the even-J contributions when the two-colour pump pulse is delayed by $T_{\rm rot}/4$ with respect to the one-colour pump, resulting in enhanced net orientation. The figure is adapted from [44].

of figure 3(c)). Besides the relative strength and separation of the two main maxima, the calculation even reproduces the appearance of a small maximum around 4.4 ps, to which we return below. The maximal degree of orientation predicted by the calculation shown in figure 3(c) amounts to $\langle \cos\theta \rangle = 0.38$ ($\zeta = 0.73$). We point out that the analysis of the high-harmonic spectra in section 4.3 yields a slightly higher value of the orientation parameter ($\zeta = 0.82$). We therefore conclude that a degree of orientation of $0.73 \leqslant \zeta \leqslant 0.82$ has been achieved.

The unusual property that orientation can be obtained at the rotational half revival rather than at the full revival can be understood by analysing the contributions from odd and even rotational states to the observed wave-packet dynamics, which is illustrated in figure 4. The interaction of a two-colour laser pulse with a molecule creates a rotational wave packet that shows net orientation (measured by $\langle \cos\theta \rangle$) only at the full rotational revival (figure 4(a)). Nevertheless, the isolated contributions from the odd- and even-J (rotational quantum number) contributions to the wave-packet dynamics show the most pronounced orientation at the rotational half revival, but modulate out of phase and thus give rise to zero net orientation. Thus enhanced orientation can be obtained by suppressing one of the two contributions at the half revival. This is achieved by a one-colour pulse, which precedes the two-colour pulse by a quarter of a rotational period. The one-colour laser pulse causes the odd- and even-J contributions to $\langle \cos^2\theta \rangle$ to modulate out of phase at the rotational quarter revival (figure 4(b)). The application of a two-colour pulse at this delay mainly orients the prealigned odd contributions to the wave-packet dynamics and thus creates enhanced net orientation at the rotational half revivals [45, 46]. By slightly detuning Δt_1 from $T_{\rm rot}/4$, it is possible to modify the odd- and even-J contributions to $\langle \cos\theta \rangle$ and to further enhance the net orientation. This aspect is experimentally investigated in the next paragraphs.

We now study the observed revival structures as a function of the two delays Δt_1 and $\Delta t_{\rm tot}$, using 30% lower intensities in both pump pulses than those quoted in section 2. Figure 5 summarizes the results in terms of both the alignment dynamics probed by an odd-harmonic order (harmonic 9, 13.9 eV, figure 5(a)) and the orientation dynamics probed by an even-harmonic order (harmonic 16, 24.8 eV, figure 5(b)). We first discuss the alignment dynamics (figure 5(a)). The signal modulation as a function of $\Delta t_{\rm tot}$ shows a maximum followed by a minimum for all Δt_1 and thus qualitatively follows the modulation of $\langle \cos^2\theta \rangle$ at the rotational half revival, where alignment precedes anti-alignment. The maximum and minimum of harmonic emission shifts linearly on the $\Delta t_{\rm tot}$ axis with increasing Δt_1. This behaviour shows that the observed alignment is dominated by the two-colour pump pulse and thus occurs for constant Δt_2.

The situation for the orientation dynamics (figure 5(b)) is different. Two main maxima are observed in the even-harmonic emission as a function of $\Delta t_{\rm tot}$. The separation of the two maxima decreases from >1 ps separation at $\Delta t_1 = 2.25$ ps to 0.5 ps separation at $\Delta t_1 = 2.0$ ps. For $\Delta t_1 = 2.0$ ps and less, a third local maximum in the even-harmonic emission arises at earlier $\Delta t_{\rm tot}$. The strongest even-harmonic emission as a function of $\Delta t_{\rm tot}$ is observed for $\Delta t_1 = 2.255$ ps.

These features can be explained by analysing the contributions from even and odd rotational levels to the observed wave-packet dynamics at different delays Δt_1 as shown in figures 5(c)–(e). Generally, the present two-pulse scheme tends to suppress the even-J contributions to the oriented wave-packet dynamics because these contributions are anti-aligned around the quarter revival (see also figure 4(b)). However, the residual orientation of the even-J contributions to the wave-packet dynamics still interferes destructively with the enhanced odd-J contributions. By precisely tuning Δt_1, we can control the magnitude of the even-J contributions to $\langle \cos\theta \rangle$, shift their extrema in time and thus control the interference between odd- and even-J contributions. The analysis for $\Delta t_1 = 1.86\,\text{ps} < T_{\rm rot}/4$ is

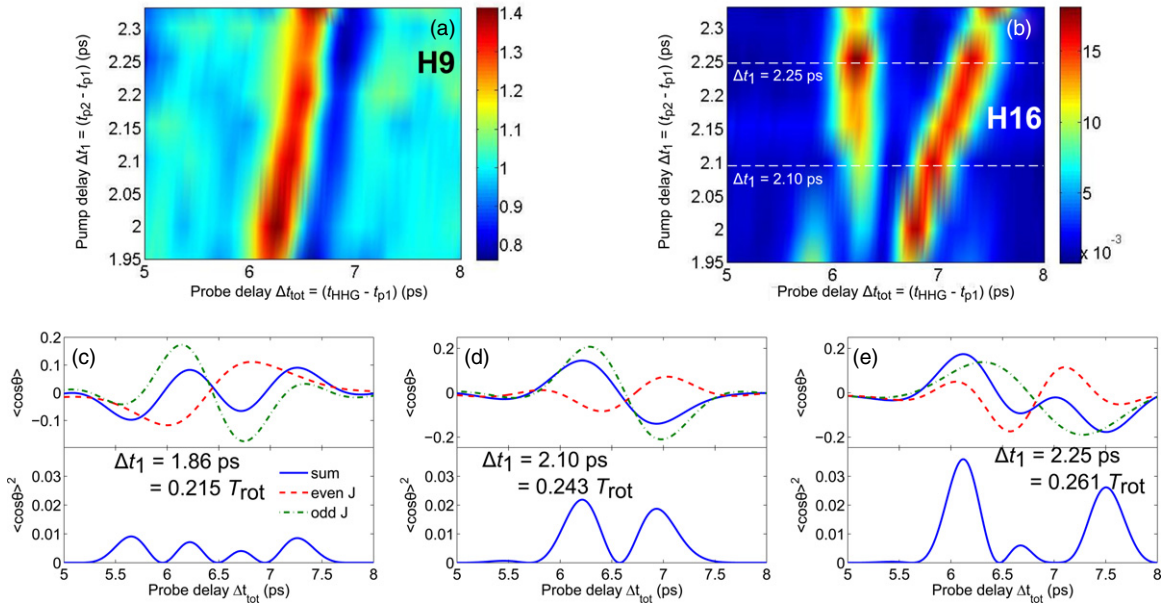

Figure 5. Three-dimensional revival maps as a function of the delay between the two pump pulses Δt_1 and as a function of the delay between the one-colour pump pulse and the probe pulse $\Delta t_{\rm tot}$. (a) Revival map of the ninth harmonic order reflecting the alignment dynamics. (b) Revival map of the 16th harmonic order reflecting the orientation dynamics. (c)–(e) Calculations of the orientation dynamics decomposed into the odd- and even-J contributions and their sum (upper panels) and plots of $\langle\cos\theta\rangle^2$ (lower panels) for three different delays Δt_1 between the two pump pulses. The delays Δt_1 for which calculations were carried out in panels (d) and (e) are marked by white dashed lines in panel (b).

shown in the upper panel of figure 5(c) decomposed into the odd-J (green dotted–dashed line) and even-J contributions (red dashed line) and their sum (solid blue line). The even-J contributions are only weakly suppressed and thus still interfere destructively with the odd-J contributions. However, the odd-J contributions show small pre- and post-orientation revivals (around 5.7 and 7.3 ps, respectively), which interfere constructively with the even-J contributions and thus create the strongest net orientation at these delays. This causes the even-harmonic emission (measured by $\langle\cos\theta\rangle^2$, lower panel) to peak at these delays as well.

For Δt_1 close to $T_{\rm rot}/4$ (figure 5(d), $\Delta t_1 = 2.10$ ps), the even-J contributions are strongly suppressed. This results in strong orientation close to the delays where the even- and odd-J contributions have their global maxima and minima, respectively. Therefore, the two maxima of the even-harmonic emission are much closer in time (lower panel of figure 5(d)). For $\Delta t_1 > T_{\rm rot}/4$ (figure 5(e), $\Delta t_1 = 2.25$ ps) the odd- and even-J contributions have again similar weights, but the pre- and post-orientation revivals of the odd-J contributions can interfere constructively with the falling and rising flanks of the even-J contributions, respectively. This gives rise to the strongest net orientation for the present parameters. Similarly as for small Δt_1, the emission maxima are separated by a longer delay (approximately 1.3 ps) compared to $\Delta t_1 \approx T_{\rm rot}/4$ because the maximum net orientation is obtained before and after the global extrema of the isolated odd- and even-J contributions to the orientation dynamics. This simulation also correctly predicts the small local maximum around $\Delta t_{\rm tot} = 6.65$ ps (corresponding to $\Delta t_2 = 4.4$ ps), which was observed experimentally in figure 3(d). This maximum arises from the global maximum of the even-J contributions to the oriented wave-packet dynamics, which interfere destructively with the odd-J contributions. The major part of the net orientation is thus extinguished and only a small fraction survives, giving rise to the weak even-harmonic emission between the two main maxima. The parameters employed in figure 5 were not optimized with respect to the degree of orientation, which is lower than in figure 3(c).

We now turn to the two-pulse orientation of oriented OCS molecules. The rotational revival structures for the even harmonics at different pump delays Δt_1 are shown in figures 6(b)–(c) and a representative revival structure for an odd-harmonic order is displayed in figure 6(a). The corresponding calculations of $\langle\cos^2\theta\rangle$ and $\langle\cos\theta\rangle^2$ are shown in figures 6(d)–(f).

The revival of the odd-harmonic order (harmonic 9, 13.9 eV) modulates in opposition to $\langle\cos^2\theta\rangle$. This is a consequence of the π-symmetry of the HOMO (highest occupied molecular orbital), which causes the photorecombination dipole moment to maximize around an alignment angle of 100° [40] causing the signal to maximize when the molecules are anti-aligned. The even-harmonic modulations follow a similar pattern as for CO. For $\Delta t_1 = 21.01$ ps (figures 6(c) and (f)), we again find two clearly separated maxima, which correspond to the two possible orientations of OCS as previously discussed and shown in figure 3(c) for the case of CO. The separation of the maxima amounts to 2.8 ps which is reproduced by the calculations (figure 6(f)). For shorter delays ($\Delta t_1 = 20.68$ ps) the maxima in the even-harmonic intensity approach each other (figure 6(b)). This trend is adequately reproduced by the calculations of $\langle\cos\theta\rangle^2$ in panel (e) for $\Delta t_1 = 20.68$ ps. However, the experimental data do not show the additional

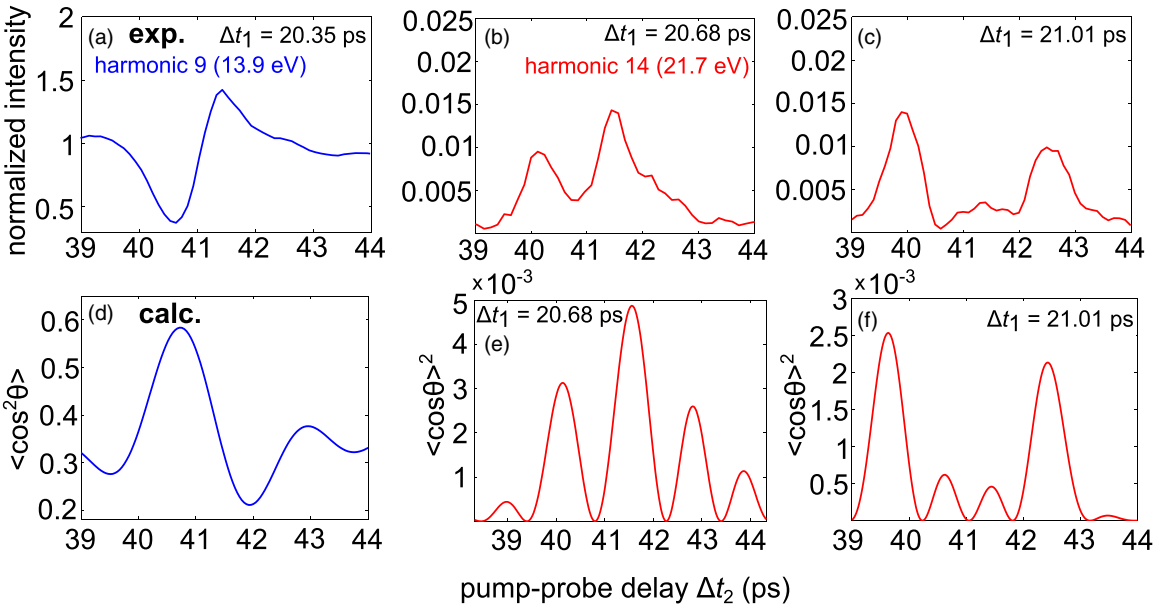

Figure 6. Observed and calculated revival structures from OCS oriented with the two-pulse scheme. (a)–(c) Revivals of various harmonic orders for different delays Δt_1 with corresponding calculations of $\langle\cos^2\theta\rangle$ and $\langle\cos\theta\rangle^2$ ((d)–(f)).

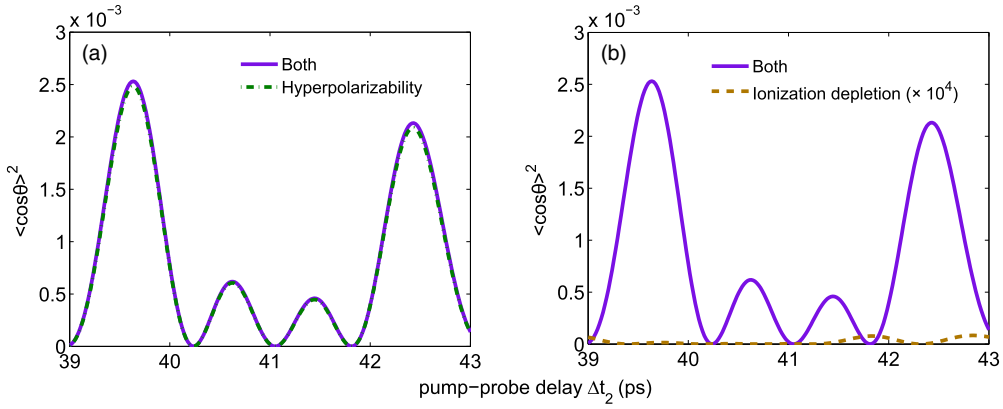

Figure 7. Mechanisms of field-free molecular orientation illustrated for OCS with a delay Δt_1 of 20.68 ps. (a) Time-evolution of $\langle\cos\theta\rangle^2$ with both mechanisms active and for the hyperpolarizability interaction only. (b) Time-evolution of $\langle\cos\theta\rangle^2$ with both mechanisms active and for the ionization-depletion mechanism only. It is clearly recognizable that the hyperpolarizability interaction is almost exclusively responsible for orientation obtained in the two-pulse scheme.

local maxima around delays Δt_2 of 39 ps, 42.8 ps and 43.7 ps that are predicted by the calculations shown in panel (e). As in the case of the two-pulse orientation studies as a function of Δt_1 and $\Delta t_{\rm tot}$ for CO (figure 5), the time evolution of $\langle\cos\theta\rangle^2$ is controlled and can be rationalized through the interference of odd- and even J-contributions which can be manipulated by tuning Δt_1.

4.2. Mechanism of the two-pulse orientation

We now analyse which mechanism is dominant in creating orientation by the two-pulse scheme: an interaction of the laser electric field with the hyperpolarizability of the molecule [31] or an ionization-depletion mechanism [42]. As described above, we calculate the evolution of $\langle\cos\theta\rangle^2$ by solving the TDSE for the coefficients $C_J^{J_0M_0}$ and selectively include a potential term in the interaction Hamiltonian describing the hyperpolarizability interaction of the molecule with the laser field (equation (3)), the interaction term accounting for the ionization depletion of the sample (equation (4)), or both. This allows us to identify the mechanism which is mainly responsible for orientation in the two-pulse scheme. Previous investigations led to the conclusion that one-pulse two-colour orientation mainly creates orientation via ionization depletion of molecules in the neutral ground state [41, 42]. In figure 7, the calculations of the two-pulse orientation of OCS for $\Delta t_1 = 20.68$ ps (figure 6(h)) are decomposed into the contributions from the hyperpolarizability (dashed–dotted green line, panel (a)) and the ionization-depletion (dashed ocher line, panel (b)) mechanism to the total orientation (solid violet line). Figure 7(a) clearly shows that practically all orientation obtained at the rotational half-revival results from the hyperpolarizability mechanism of orientation, whereas the ionization-depletion mechanism (figure 7(b)) has a negligible contribution. The same conclusion was reached in the case of CO as described in [44].

The reason that the ionization-depletion mechanism cannot be enhanced at the rotational half revival is that the contributions of the odd and even J-levels to the total rotational dynamics exhibit practically no orientation at the rotational half revival, which makes it impossible to obtain enhanced net orientation at the rotational half revival by the ionization-depletion mechanism with the present two-pulse scheme.

Thus, the present two-pulse scheme for field-free molecular orientation is the only presently known completely field-free technique, which creates macroscopic degrees of orientation without ionizing major parts of the sample. This makes it an ideal technique for all detection schemes which suffer from substantial ionization. Although the intensities used in the present study ionized a small fraction of the sample, the hyperpolarizability interaction scales with $\gamma E^3(t)$ in contrast to the exponential dependence of the ionization-depletion mechanism, which means that high degrees of orientation can still be reached with the hyperpolarizability mechanism at lower non-ionizing intensities. This is a crucial point whenever high particle densities are required, as is the case for high-harmonic and attosecond spectroscopies, but also for coincidence techniques and other probing schemes which suffer from space-charge limitations.

4.3. High-harmonic spectroscopy of electronic structure

This section outlines our general approach to obtaining electronic-structure information and the degree of orientation from high-harmonic spectra of polar molecules. We start by calculating the odd-harmonic spectrum of an oriented ensemble of molecules according to equation (9) using the symmetrized axis distribution, according to equation (17). Subsequently, the even-harmonic spectrum is predicted with an anti-symmetrized axis distribution (equation (18)) that vanishes in the absence of orientation. The only unknown parameter in this simplified approach is the degree of orientation η (or ζ) as defined in section 3.2.

In this section, we focus on the high-harmonic spectra of CO (figure 3(a)). We determine the degree of orientation in a first step. We then provide an explanation for an observed intensity maximum in the even-harmonic emission, which reflects a shape resonance of the continuum electron encoded in the photorecombination dipole moment.

A first very rough estimate of the degree of orientation can be obtained from the ratio of the even-harmonic intensities to the mean intensity of the two adjacent odd-harmonic orders [41]. When all molecule-specific quantities, such as ionization rates, recombination dipole moments etc are ignored, this ratio is proportional to the squared degree of orientation η^2. In two-pulse orientation experiments on CO, we obtain an average value of $I_{\mathrm{even}}/I_{\mathrm{odd}} = 0.44$ for the harmonic orders 12–24 (18.6 eV–37.2 eV), which gives an estimate of $\eta = 0.66$, i.e. $\zeta = 0.83$. This improves the degree of field-free orientation compared to its first demonstration [39] by a factor of $\sim$15 and compared to previous high-harmonic studies of oriented molecules [40, 41] by a factor of > 3.

A more reliable method to estimate the degree of orientation [41] consists in simulating the odd-harmonic spectrum according to equation (9). The resulting even-harmonic spectrum for $\eta = 0.65$ (i.e. $\zeta = 0.82$) is shown in figure 8(a), which gives the best agreement with the observed experimental intensities. We thus find a probably fortuitous agreement between the two methods in the present case.

We now take a closer look at the spectral intensity profile of the emitted harmonics (figure 8(a)). A maximum at harmonic 18 (27.9 eV) is visible in the even-to-odd intensity ratio. The envelope of the odd-harmonic spectrum does however not display any such feature and monotonically decreases until the cutoff. To explain these spectral features, we first consider the photorecombination dipole amplitudes shown in figure 8(b), which indeed show a strong maximum between the 17th and 20th harmonic order. This maximum reflects a shape resonance, which has been observed using unaligned molecules in the partial photoionization cross section corresponding to the $X\,^2\Sigma^+$ state of CO^+ at 23.6 eV [65].

The crucial question which now arises is why this maximum is only visible in the even-harmonic emission, but not in the odd-harmonic spectrum. In order to answer this question, it is important to realize that in contrast to photoelectron spectroscopy, high-harmonic spectra are sensitive to the coherent average of emissions from molecules aligned under different angles. This means that the angle-dependent phases of the photorecombination dipole moment and the contribution from the Stark effect both play a crucial role.

The phase of the photorecombination dipole moment is displayed in figure 8(c) and the Stark phase is shown in figure 8(d). An expression for the Stark phase was given in equation (10). The phase contributed by the linear Stark effect has been shown to depend only on the molecular properties and the emitted photon energy [57]. The Stark phase depends on the molecular orientation with respect to the polarization of the laser field, the ionization potential and the difference between the permanent dipole moments of the molecule in the relevant ionic and neutral states (i.e. the permanent dipole moment of the ionized orbital in the single-active-electron approximation). We plot the Stark phase as a function of the alignment angle and harmonic order in figure 8(d) using a dipole moment of 1.1287 au [56] for HOMO. For the two possible parallel orientations of the molecule, the Stark phase varies by 1.5 rad in total magnitude as a function of the displayed harmonic orders. For intermediate angles, the phase variation is smaller. This additional phase contribution is added to the phase of the recombination dipole moment. The resulting total phase is shown in figure 8(e). The Stark phase visibly modifies the phase profile of the photorecombination matrix elements (figure 8(c)). Most importantly, the Stark-phase contribution decreases the asymmetry of the phase of the photorecombination dipole moment. This aspect is illustrated in panel (f), where the difference between the phase of emission for recombination from the oxygen- versus the carbon-side of the molecule is displayed. We show calculations including the Stark-phase contribution (solid black line) and neglecting it (dashed–dotted magenta line). The phase difference between the two recollision sides is almost exactly

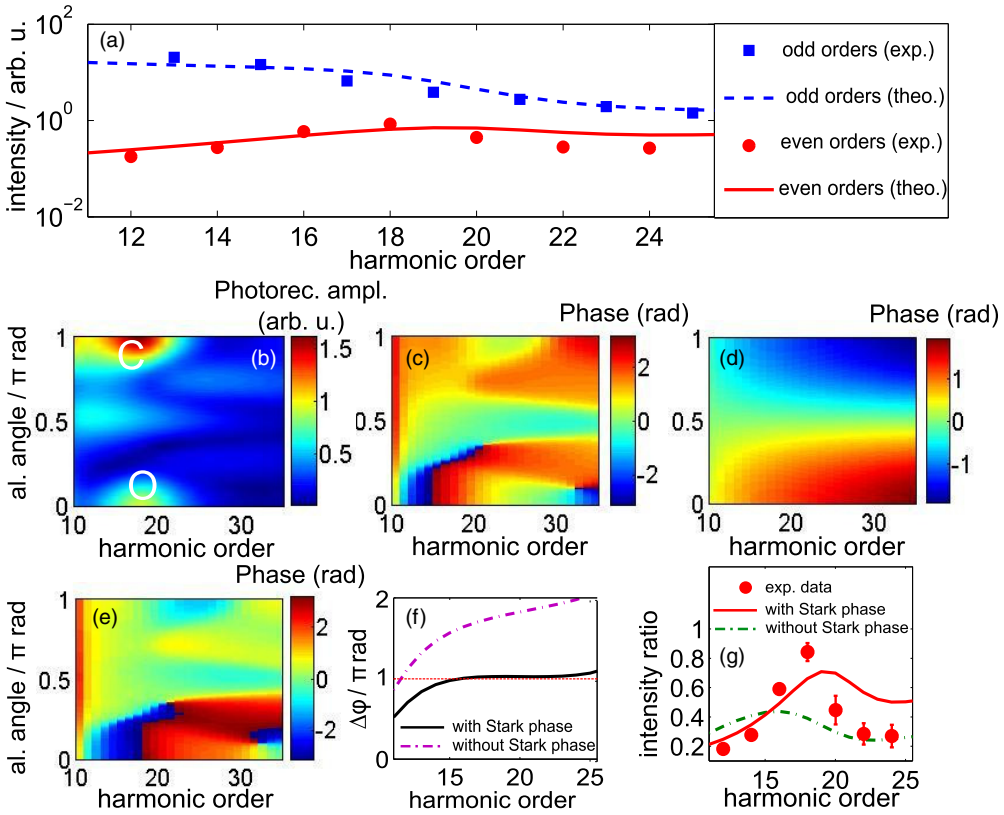

Figure 8. Calculation of the high-harmonic spectra of oriented CO molecules. (a) Experimental and simulated intensity envelopes of the odd-harmonic orders and of the even-to-odd ratio. The experimental error bars lie within the width of the markers. (b) Calculated amplitude of the photorecombination matrix elements as a function of the alignment angle θ and harmonic order for an electron recombining from the positive side of the z-axis shown in figure 2(e). (c) Calculated phase of the photorecombination matrix elements. (d) Phase contribution from the Stark effect. (e) Sum of the phase contributions from the photorecombination matrix element and the Stark effect (equation (10)). (f) Phase difference between recombination from opposite sides of the molecule (0 and π rad) with and without the Stark-phase contribution. (g) Simulated even-to-odd ratio with and without the Stark-phase contribution shown together with the experimental ratio. The error bars represent a 95% confidence interval with standard deviations estimated from the signal fluctuations of the isotropic sample.

π for harmonic orders 16–22 when the Stark phase is taken into account, whereas it sharply increases from π towards 2π over the same range when the Stark phase is neglected. We recall that a phase difference of π causes the even harmonics to be enhanced according to equation (13), while the odd harmonics are suppressed (equation (12)). This is precisely the reason, why the intensity envelope of the even harmonics reflects the shape resonance while that of the odd orders does not.

For the sake of comparison, the experimental even-to-odd ratio is shown in figure 8(g) together with the calculations including (solid red line) or neglecting (dashed–dotted green line) the Stark-phase contribution. While the calculation including the Stark-phase contribution adequately captures the position of the emission maximum and the general shape of the even-to-odd ratio, the calculation without the Stark phase predicts a maximum at too low photon energies (around harmonic 14–16) and shows a generally worse agreement with the experiment. The maximum occurs at too low photon energies when the Stark phase is omitted because the total phase difference already crosses π around harmonic 12 and thus causes a constructive interference at lower photon energies than experimentally observed. A more sophisticated model taking into account contributions from electronically excited states of the cation to the high-harmonic emission provides a more quantitative agreement between theory and experiment and will be published elsewhere.

These results show that high-harmonic spectra of polar molecules reveal additional details of electronic-structure information compared to non-polar molecules. The position where shape resonances or Cooper-type minima [21, 22, 27, 44, 66] appear in high-harmonic spectra of polar molecules are additionally affected by the Stark phase. Moreover, the resonances or minima may appear in the even-harmonic spectra, the odd-harmonic spectra or both and the position in the two types of spectra may in general differ. Consequently, by comparing such observables in HHS and photoionization spectroscopies, new insights can be obtained into both phase and amplitude asymmetries in photoionization and photorecombination or additional laser-field-induced effects.

5. Conclusion

In this article, two-pulse orientation was established as a powerful method for orienting molecules at high densities in the absence of external fields. Two-pulse orientation provides the highest degrees of completely field-free orientation (73–82% of CO molecules pointing in the same direction) reported so far. We have explored the mechanisms creating

orientation by this scheme and found that two-pulse orientation offers macroscopic degrees of field-free molecular orientation without ionizing major parts of the sample. We rationalized the oriented wave-packet dynamics by investigating the odd- and even-J contributions to the orientation dynamics and demonstrated control over the orientation dynamics by tuning the delay between the one-colour alignment and the two-colour orientation pulses. Finally, we demonstrated how the measured high-harmonic spectra can be simulated from first principles and how the degree of orientation can be estimated from the spectra. The calculations of the high-harmonic spectra of CO allowed us to relate an observed intensity maximum in the even-harmonic emission to a shape resonance which is absent from the odd-harmonic spectrum as a result of a sub-cycle Stark effect, generic for polar molecules.

Acknowledgments

We gratefully acknowledge funding from the Swiss National Science Foundation (PP00P2_128274) and ETH Zürich (ETH-33 10-3).

References

[1] Krausz F and Ivanov M 2009 Attosecond physics *Rev. Mod. Phys.* **81** 163
[2] Goulielmakis E *et al* 2010 Real-time observation of valence electron motion *Nature* **466** 739
[3] Wörner H J and Corkum P B 2011 Imaging and controlling multielectron dynamics by laser-induced tunnel ionization *J. Phys. B: At. Mol. Opt. Phys.* **44** 041001
[4] Fleischer A, Wörner H J, Arissian L L, Liu L R, Meckel M M, Rippert A A, Dörner R, Villeneuve D M, Corkum P B and Staudte A 2011 Probing angular correlations in sequential double ionization *Phys. Rev. Lett.* **107** 113003
[5] Sansone G *et al* 2010 Electron localization following attosecond molecular photoionization *Nature* **465** 763
[6] Kraus P M, Zhang S B, Gijsbertsen A, Luchhese R R, Rohringer N and Wörner H J 2013 High-harmonic probing of electronic coherence in dynamically aligned molecules *Phys. Rev. Lett.* **111** 243005
[7] Cederbaum L S and Zobeley J 1999 Ultrafast charge migration by electron correlation *Chem. Phys. Lett.* **307** 205
[8] Breidbach J and Cederbaum L S 2003 Migration of holes: Formalism, mechanisms and illustrative applications *J. Chem. Phys.* **118** 3983
[9] Kraus P M, Rupenyan A, Schneider J, Baykusheva D and Wörner H J 2013 Probing attosecond charge migration in oriented molecules *4th Int. Conf. on Attosecond Physics* (http://atto2013.celia.u-bordeaux1.fr/index.php/invited-speakers)
[10] Drescher M, Hentschel M, Kienberger R, Uiberacker M, Yakolev V, Scrinzi A, Westerwalbesloh T, Kleineberg U and Krausz F 2002 Time-resolved atomic innershell spectroscopy *Nature* **419** 803
[11] Schultze M *et al* 2010 Delay in photoemission *Science* **328** 1658
[12] Paul P M, Toma E S, Breger P, Mullot G, Augé F, Balcou Ph, Muller H G and Agostini P 2001 Observation of a train of attosecond pulses from high harmonic generation *Science* **292** 1689
[13] Klünder K *et al* 2011 Probing single-photon ionization on the attosecond time scale *Phys. Rev. Lett.* **106** 143002
[14] Eckle P, Pfeiffer A N, Cirelli C, Staudte A, Dörner R, Muller H G, Büttiker M and Keller U 2008 Attosecond ionization and tunneling delay time measurements in helium *Science* **322** 1525
[15] Pfeiffer A N, Cirelli C, Smolarski M, Dörner R and Keller U 2011 Timing the release in sequential double ionization *Nature Phys.* **7** 428
[16] Stapelfeldt H and Seideman T 2003 Aligning molecules witht strong laser pulses *Rev. Mod. Phys.* **75** 543
[17] Bisgaard C Z, Clarkin O J, Wu G, Lee A M D, Gessner O, Hayden C C and Stolow A 2009 Time-Resolved Molecular Frame Dynamics of Fixed-in-space CS2 Molecules *Science* **323** 1464
[18] Meckel M *et al* 2008 Laser induced electron tunnelling and diffraction *Science* **320** 1478–82
[19] Okunishi M, Niikura H, Lucchese R R, Morishita T and Ueda K 2011 Extracting electron-ion differential scattering cross sections for partially aligned molecules by laser-induced rescattering photoelectron spectroscopy *Phys. Rev. Lett.* **106** 063001
[20] Itatani J, Levesque J, Zeidler D, Niikura H, Pépin H, Kieffer J C, Corkum P B and Villeneuve D M 2004 Tomographic imaging of molecular orbitals *Nature* **432** 867
[21] Wörner H J, Niikura H, Bertrand J B, Corkum P B and Villeneuve D M 2009 Observation of electronic structure minima in high-harmonic generation *Phys. Rev. Lett.* **102** 103901
[22] Shiner A D, Schmidt B, Trallero-Herrero C, Wörner H J, Patchkovskii S, Corkum P B, Kieffer J-C, Légaré F and Villeneuve D M 2011 Probing collective multi-electron dynamics in xenon with high-harmonic spectroscopy *Nature Phys.* **7** 464
[23] Vozzi C, Negro M, Calegari F, Sansone G, Nisoli M, De Silvestri S and Stagira S 2011 Generalized molecular orbital tomography *Nature Phys.* **7** 822
[24] McFarland B K, Farrell J P, Bucksbaum P H and Gühr M 2008 High harmonic generation from multiple orbitals in N_2 *Science* **322** 1232
[25] Haessler S *et al* 2010 Attosecond imaging of molecular electronic wavepackets *Nature Phys.* **6** 200
[26] Wörner H J, Bertrand J B, Hockett P, Corkum P B and Villeneuve D M 2010 Controlling the interference of multiple molecular orbitals in high-harmonic generation *Phys. Rev. Lett.* **104** 233904
[27] Rupenyan A, Bertrand J B, Villeneuve D M and Wörner H J 2012 All-optical measurement of high-harmonic amplitudes and phases in aligned molecules *Phys. Rev. Lett.* **108** 033903
[28] Rupenyan A, Kraus P M, Schneider J and Wörner H J 2013 High-harmonic spectroscopy of isoelectronic molecules: Wavelength scaling of electronic-structure and multielectron effects *Phys. Rev.* A **87** 033409
[29] Rupenyan A, Kraus P M, Schneider J and Wörner H J 2013 Quantum interference and multielectron effects in high-harmonic spectra of polar molecules *Phys. Rev.* A **87** 031401
[30] Friedrich B and Herschbach D R 1991 Spatial orientation of molecules in strong electric fields and evidence for pendular states *Nature* **353** 412
[31] Sakai H, Minemoto S, Nanjo H, Tanji H and Suzuki T 2003 Controlling the orientation of polar molecules with combined electrostatic and pulsed, nonresonant laser fields *Phys. Rev. Lett.* **90** 083001
[32] Goban A, Minemoto S and Sakai H 2008 Laser-field-free molecular orientation *Phys. Rev. Lett.* **101** 013001
[33] Holmegaard L, Nielsen J H, Nevo I and Stapelfeldt H 2009 Laser-induced alignment and orientation of quantum-state-selected large molecules *Phys. Rev. Lett.* **102** 023001

[34] Holmegaard L *et al* 2010 Photoelectron angular distributions from strong-field ionization of oriented molecules *Nature Phys.* **6** 428
[35] Ghafur O, Rouzée A, Gijsbertsen A, Siu W K, Stolte S and Vrakking M J J 2009 Impulsive orientation and alignment of quantum-state-selected NO molecules *Nature Phys.* **5** 289
[36] Vrakking M J J and Stolte S 1997 Coherent control of molecular orientation *Chem. Phys. Lett.* **271** 209
[37] Kanai T and Sakai H 2001 Numerical simulations of molecular orientation using strong, nonresonant, two-color laser fields *J. Chem. Phys.* **115** 5492
[38] Oda K, Hita M, Minemoto S and Sakai H 2010 All-optical molecular orientation *Phys. Rev. Lett.* **104** 213901
[39] De S *et al* 2009 Field-free orientation of CO molecules by femtosecond two-color laser fields *Phys. Rev. Lett.* **103** 153002
[40] Kraus P M, Rupenyan A and Wörner H J 2012 High-harmonic spectroscopy of oriented OCS molecules: emission of even and odd harmonics *Phys. Rev. Lett.* **109** 233903
[41] Frumker E, Hebeisen C T, Kajumba N, Bertrand J B, Wörner H J, Spanner M, Villeneuve D M, Naumov A and Corkum P B 2012 Oriented rotational wave-packet dynamics studies via high harmonic generation *Phys. Rev. Lett.* **109** 113901
[42] Spanner M, Patchkovskii S, Frumker E and Corkum P B 2012 Mechanisms of two-color laser-induced field-free molecular orientation *Phys. Rev. Lett.* **109** 113001
[43] Goll E, Wunner G and Saenz A 2006 Formation of ground-state vibrational wave packets in intense ultrashort laser pulses *Phys. Rev. Lett.* **97** 103003
[44] Kraus P M, Baykusheva D and Wörner H J 2013 Field-free molecular orientation with a bipulse scheme probed by high-harmonic spectroscopy http://arxiv.org/abs/1311.3923
[45] Zhang S, Lu C, Jia T, Wang Z and Sun Z 2011 Controlling field-free molecular orientation with combined single- and dual-color laser pulses *Phys. Rev.* A **83** 043410
[46] Tehini R, Hoque Md Z, Faucher O and Sugny D 2012 *Phys. Rev.* A **85** 043423
[47] Spanner M and Patchkovskii S 2009 One-electron ionization of multielectron systems in strong nonresonant laser fields *Phys. Rev.* A **80** 063411
[48] Tolstikhin O I, Morishita T and Madsen L B 2011 Theory of tunneling ionization of molecules: Weak-field asymptotics including dipole effects *Phys. Rev.* A **84** 053423
[49] Madsen L B, Tolstikhin O I and Morishita T 2012 Application of the weak-field asymptotic theory to the analysis of tunneling ionization of linear molecules *Phys. Rev.* A **85** 053404
[50] Madsen L B, Jensen F, Tolstikhin O I and Morishita T 2013 Structure factors for tunneling ionization rates of molecules *Phys. Rev.* A **87** 013406
[51] Linstrom P and Mallard E W G 2013 *NIST Chemistry WebBook, NIST Standard Reference Database Number 69* (Gaithersburg, MD: NIST) http://webbook.nist.gov
[52] Peterson K A and Dunning T H Jr 1997 The CO molecule: the role of basis set and correlation treatment in the calculation of molecular properties *J. Mol. Struct.* **400** 93
[53] Wang L-S, Reutt J E, Lee Y T and Shirley D A 1988 High resolution UV photoelectron spectroscopy of CO_2^+, COS^+ and CS_2^+ using supersonic molecular beams *J. Electron Spectrosc. Relat. Phenom.* **47** 167
[54] Maroulis G and Menadakis M 2010 Polarizability and hyperpolarizability of ocs and N_2O *Chem. Phys. Lett.* **494** 144
[55] Lewenstein M, Balcou P, Ivanov M Y, L'Huillier A and Corkum P B 1994 Theory of high-harmonic generation by low-frequency laser fields *Phys. Rev.* A **49** 2117
[56] Etches A and Madsen L B 2010 Extending the strong-field approximation of high-order harmonic generation to polar molecules: gating mechanisms and extension of the harmonic cutoff *J. Phys. B: At. Mol. Opt. Phys.* **43** 155602
[57] Etches A, Gaarde M B and Madsen L B 2012 Laser-induced bound-state phases in high-order-harmonic generation *Phys. Rev.* A **86** 023818
[58] Corkum P B 1993 Plasma perspective on strong field multiphoton ionization *Phys. Rev. Lett.* **71** 1994
[59] Gianturco F A, Lucchese R R and Sanna N 1994 Calculation of low-energy elastic cross sections for electron-CF_4 scattering *J. Chem. Phys.* **100** 6464
[60] Natalense A P P and Lucchese R R 1999 Cross section and asymmetry parameter calculation for sulfur 1s photoionization of SF_6 *J. Chem. Phys.* **111** 5344
[61] Dudovich N, Smirnova O, Levesque J, Ivanov M, Villeneuve D M and Corkum P B 2006 Measuring and controlling the birth of attosecond pulses *Nature Phys.* **2** 781
[62] Li H, Ray D, De S, Znakovskaya I, Cao W, Laurent G, Wang Z, Kling M F, Le A T and Cocke C L 2011 Orientation dependence of the ionization of CO and NO in an intense femtosecond two-color laser field *Phys. Rev.* A **84** 043429
[63] Zhang B, Yuan J and Zhao Z 2013 Dynamic core polarization in strong-field ionization of CO molecules *Phys. Rev. Lett.* **111** 163001
[64] Pavičić D, Lee K F, Rayner D M, Corkum P B and Villeneuve D M 2007 Direct measurement of the angular dependence of ionization for N_2, O_2, and CO_2 in intense laser fields *Phys. Rev. Lett.* **98** 243001
[65] Plummer E W, Gustafsson T, Gudat W and Eastman D E 1977 Partial photoionization cross sections of N_2 and CO using synchrotron radiation *Phys. Rev.* A **15** 2339
[66] Ren X, Makhija V, Le A-T, Troß J, Mondal S, Jin C, Kumarappan V and Trallero-Herrero C 2013 Measuring the angle-dependent photoionization cross section of nitrogen using high-harmonic generation *Phys. Rev.* A **88** 043421